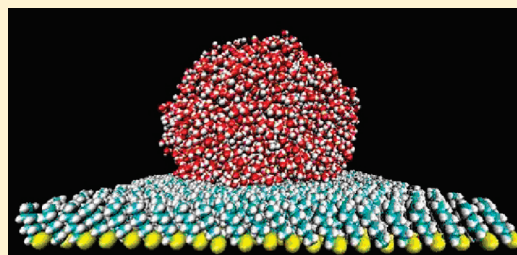


Molecular Simulations of the Structure and Dynamics of Water Confined between Alkanethiol Self-Assembled Monolayer Plates

Joshua P. Layfield and Diego Troya*

Department of Chemistry, Virginia Tech, 107 Davidson Hall, Blacksburg, Virginia 24061-0212, United States

ABSTRACT: We have studied structural and dynamic properties of water confined between hydrophobic alkanethiol self-assembled monolayers (SAMs) using molecular-dynamics simulations. After quantifying the hydrophobic nature of the SAM surfaces via contact-angle calculations involving water droplets, we analyze the effect that the hydrophobic surfaces have on structural properties of the confined water such as density, tetrahedral ordering, orientational structure at the SAM–water interface, and on dynamical properties via calculation of diffusion coefficients. Both the SPC/E and TIPSP water models have been utilized in the calculations. All of the analyses of the structure and dynamics of water are performed as a function of separation from the surface with a focus on determining the range of the effect of hydrophobic surfaces on the water film. We show that the effects of the surface are not noticeable at water-film depths of approximately 1 nm for the structural properties examined. However, calculated diffusion coefficients in the plane of the surface indicate the SAMs induce enhancement of water motion clearly beyond 1 nm. While the enhanced lateral diffusion coefficients persist into deeper regions of the water film than any other measure of the hydrophobic effect examined in this work, the range of influence of the surface on the dynamics of water falls dramatically short of the range for hydrophobic interactions measured in some experiments.



INTRODUCTION

The interactions experienced by hydrophobic species in an aqueous environment have wide-ranging implications in a variety of fields. Many phenomena related to essential biological processes are dominated by the properties of water confined in hydrophobic environments. For instance, hydrophobic amino acid residues appear prominently in protein-folding mechanisms in aqueous environments.^{1–3} Moreover, nonpolar pockets in proteins have been shown to be responsible for protein stability over a tremendous range of pressures (up to 2000 atm)^{4,5} and temperatures (up to 400 K).⁶ In fact, the nonpolar regions in the native conformations of membrane proteins on thermophilic bacteria facilitate optimal cellular growth under extreme conditions.⁷ Furthermore, it has been recently shown that intervening thin films of water between hydrophobic surfaces are crucial to the adhesion of the spatulae of geckos to many different chemical substrates.⁸ Additionally, Kalra et al. have recently shown the role that intervening water films play in reducing friction at the molecular level.⁹

The mutual structural and dynamic effects that water and hydrophobic surfaces have on one another have lent themselves to extensive experimental and theoretical investigation. The first direct experimental evidence of the length scale and magnitude of the interaction between hydrophobic surfaces in water was shown by Israelachvili and Pashley in 1982,¹⁰ who reported an attractive force acting at distances as long as 10–15 nm. A subsequent key study by Parker et al.¹¹ showed that the magnitude of the attraction between hydrophobic surfaces in water is much larger than what predicted from models solely accounting for

electrostatic and van der Waals forces acting between the two surfaces.^{12,13} The inability of traditional intersurface force models to reproduce the strength and range of the hydrophobic interaction led to the conclusion that the effects that solute and solvent have on one another need to be explicitly considered.

More recently, a large number of studies using modern surface force apparatus (SFA) and atomic force microscopy (AFM) techniques have measured hydrophobic attraction at surface separation distances ≥ 100 nm.^{14–34} While there are numerous experimental accounts of the strength and range of the hydrophobic interaction, a definitive mechanism for the measured long-range attraction has not been confirmed. The difficulty in unequivocally determining the mechanism of the interaction is due in part to the dramatic dependence of the force on the type of hydrophobic surface present. For instance, the type of binding of the surfactant molecules to the substrate (covalent bonding vs physisorption) seems to have a major effect on the hydrophobic interaction.³⁵

Some of the major mechanisms proposed to describe the attraction of hydrophobic plates in water include (1) capillary evaporation of the intervening water film, which leads to collapse of the cavity between the plates,³⁶ (2) turbulent and unstable water forming gaseous bubbles that bridge the surfaces and serve as precursor states for complete evaporation as the surfaces approach one another,¹¹ and (3) increased water structuring

Received: December 17, 2010

Revised: March 16, 2011

Published: April 05, 2011

induced by hydrophobic confinement, which results in attraction between the confining surfaces.³⁷

To illuminate the mechanism involved in the long-range interaction between surfaces in aqueous environments and investigate the nature of the confined water, extensive work has been done using molecular-dynamics (MD) simulations. While recent simulations have focused on the simulation of water confined near realistic, atomistic hydrophobic surfaces, seminal MD investigations focused on nonatomistic hydrophobic plates that were modeled as Lennard-Jones particles. These studies provided important insight into the role that confining surfaces play in the hydrophobic interaction.^{38,39}

The simulations clearly reveal that the strength of solvent–solute interactions control the properties of solvent molecules near the surface. Strong water–surface interactions, such as those afforded by a hydrophilic surface with hydrogen-bonding moieties, result in complete and persistent hydration of the surface.^{40–42} On the other hand, a gaseous depletion layer is formed when solvent–surface interactions are weaker than the solvent self-interactions, such as is the case in hydrophobic surfaces.³⁸ This depletion layer stands in stark contrast to the distorted hydrogen-bonding structure exhibited around small hydrophobic solutes, such as clathrate hydrates.^{43,44} Solutes with a radius of curvature $< \sim 1$ nm, exhibit this type of structure, whereas larger solutes or extended surfaces induce the dry interfaces.⁴⁵ The presence of a depletion region and the resulting water density layering do not seem to correlate directly with the degree of hydrophobicity of a surface. For instance, Garde and co-workers have shown that the width of the depletion layer does not follow the trend seen in the water contact angles on the surface, which is a traditional experimental measure of hydrophobicity.⁴⁶ Instead, these authors have shown that solvent compressibility at the interface is much more strongly correlated with hydrophobicity, as measured by water density fluctuations at the interface in MD simulations.

In an effort to characterize the proposed capillary-evaporation mechanism for hydrophobic attraction, Huang et al. suggested that the critical distance at which capillary evaporation of the intervening water film occurs (dewetting) depends on the cross sectional area and shape of such hydrophobic plates.³⁶ This result is important because atomistic simulations can rarely tackle the hydrophobic-plate sizes used in macroscopic experiments.

More recent work studying water confined near flat hydrophobic surfaces demonstrates the influence that the walls have on the intervening water film. Kumar et al. show that for a 1.1 nm thick film there are fewer hydrogen bonds at the interface than in bulk water, and the water phase diagram is shifted in a way that is analogous to raising the temperature by 40 K.⁴⁷ They also show that water at the solid–liquid interface shows slightly enhanced translational dynamics compared to water at the center of the thin film.

Making the transition from smooth interfaces to more physically realistic surfaces has also been an active area of study. Scheidler et al. show that at smooth interfaces the structural relaxation time decreases for a simple liquid compared to bulk values, and that the exact opposite is true for atomically rough interfaces.⁴⁸ More recently, Hummer and co-workers have shown that given a constant interaction potential, an interface can transition from hydrophilic to hydrophobic with increasing roughness.⁴⁹

The emerging picture for the nature of water–surface interfaces includes the strong interplay between surface potential,

topography, and heterogeneity. To this end, Giovambattista et al. have recently contributed a series of papers describing the effects that pressure, temperature, and surface topology have on the critical dewetting distance for water in between two silica-based hydrophobic plates.^{50–52} The calculations show that as the temperature increases and the external pressure decreases, the critical dewetting distance becomes longer. At pressures of 1 bar and 300 K, the largest intersurface separation at which dewetting is observed in the simulations is less than 0.8 nm during the simulation times studied, which are all at most 1 ns. This body of work also indicated that water at distances larger than just 1 nm from a hydrophobic surface showed behavior that was indistinguishable from bulk water, based on the metrics analyzed.

As the forces determined in the experiments exist on much longer distances (up to 100 nm) than the simulations predict, a dewetting mechanism such as the one pursued in the simulations does not seem to be solely responsible for the hydrophobic effect. Other signatures that distinguish water confined between hydrophobic surfaces and bulk water ought to extend well beyond the range seen in the simulations mentioned above. In this work, we show the results of MD calculations of hydrophobic surfaces submerged in water with the goal of identifying the properties of confined water that might be responsible for the long-range force measured between hydrophobic surfaces in the experiment. To this end, our simulations have been performed on water films of thickness (up to 5.5 nm) substantially larger than in previous work.

The rest of this article is organized as follows. First, we discuss the computational methods employed in this work. We then show the analysis of the structure and dynamics of water confined near hydrophobic SAM surfaces and offer concluding remarks.

■ SIMULATION DETAILS

In an attempt to model realistic hydrophobic surfaces, we have employed in all of our simulations alkanethiolate self-assembled monolayers (SAMs), which are commonly used in experiment to hydrophobize gold surfaces. The SAM surfaces are composed of hexanethiolate molecules arranged in a hexagonal pattern with an interchain spacing of 4.98 Å and a chain tilt angle of 30°. These SAM conditions correspond to the experimental equilibrium conditions of a SAM surface on a Au(111) surface.⁵³ The forces acting on all of the SAM atoms are described by the all-atom version of the OPLS force field.⁵⁴ Our choice of this force field was informed by its satisfactory reproduction of the experimental tilt angle of the alkanethiol SAM surfaces on gold ($\sim 30^\circ$),⁵⁵ and its use in prior work.^{46,56,57} We show below that the force field used in the simulations reproduces the water contact angle obtained in other work with other potentials, lending confidence to its adequacy.

In the simulations, two SAM surfaces are placed opposed to each other and along the *xy*-plane. Typical SAM surfaces are composed of 15×15 alkanethiolate chains that result in surface areas of 6.5×7.5 nm². The separation between the two surfaces, and thus the thickness of the intervening water film, can be controlled by modifying the coordinates of the surface atoms along the *z*-axis only. In this work, we have varied the thickness of the intersurface water film from 0.8 to 5.5 nm. Periodic images of the SAM surfaces in the *x*-axis are separated by ~ 2 nm reservoirs of water, which are not included in the analysis. Instead, the analysis of the structure and dynamics of water presented below has been performed for only those molecules of water in between

the alkane regions of the surfaces. For convenience, the size of the simulation box in the y direction is commensurate with the SAM so that, with periodic boundary conditions, an infinite surface is created along this axis. Including another water reservoir also along this direction did not affect the results presented below.

All of our simulations have been performed using the GRO-MACS molecular dynamics program.⁵⁸ The long-range Coulombic interactions are modeled using the particle mesh Ewald (PME) sum technique with a cutoff distance of 1.0 nm.⁵⁹ To facilitate the simulations, the positions of the non-hydrogen atoms of the SAM surfaces were restrained by a force constant of $1000 \text{ kJ mol}^{-1} \text{ nm}^{-2}$ using the LINear Constraint Solver (LINCS) algorithm,⁶⁰ also implemented in GROMACS. Most of the MD simulations were performed in a semi-isotropic NPT ensemble in which the pressure was controlled by a Berendsen barostat,⁶¹ which maintained the external pressure at 1 bar along the x -direction (the lengths of the simulation box were frozen along the y - and z -axes). The atomic velocities were rescaled over the course of each MD simulation to maintain target temperatures.⁶² Sample simulations were repeated by using a Nose–Hoover thermostat and the results were indistinguishable from the ones reported here. A subset of calculations were performed in the NVT ensemble with an average water density of 1 g/cm^3 to check the generality of the results presented in this work. The molecular dynamics simulations were performed with a time step of 2 fs, and the atomic coordinates were printed every 1 ps for analysis. Typical simulation times were 10 ns, but the results presented herein have been verified for 20 ns sample simulations and in limited cases up to $0.1 \mu\text{s}$. The specific details of the each simulation are presented in the text and figure captions.

The water confined between the SAM plates has been represented using two different models of water, SPC/E⁶³ and TIPSP.⁶⁴ A major difference between the two water models that is pertinent to the work presented here is in their description of the liquid–solid phase transition. While the SPC/E water model is less computationally demanding and has a slightly more accurate bulk density around 300 K, its predicted melting point at ambient pressure is $213 \pm 6 \text{ K}$.⁶⁵ The TIPSP method requires more computational expense because it explicitly models the two lone pairs located on the oxygen atom in addition to all three atomic centers, but it yields a more reasonable melting point of $271 \pm 2 \text{ K}$. This phase-transition behavior is important because one of the aims of this work is to establish the temperature dependence of some of the structural and dynamical properties of confined water. Our calculations using both models will thus help us verify that the changes seen in water behavior are a consequence of confinement and not an anomaly of a particular water model.

RESULTS

A. Contact Angle. Sakamoto et al.⁶⁶ and Zhang et al.⁶⁷ have both independently shown that surfaces covered with long-chain surfactant molecules exhibit greater attraction in water than surfaces coated with shorter-chain surfactants. All current experiments agree that the more hydrophobic a surface, the greater the magnitude of the attraction in both AFM and SFA experiments. However, quantification of the absolute or even relative hydrophobicity of different surfaces is nontrivial and has warranted extensive study in the past.^{46,68,69}

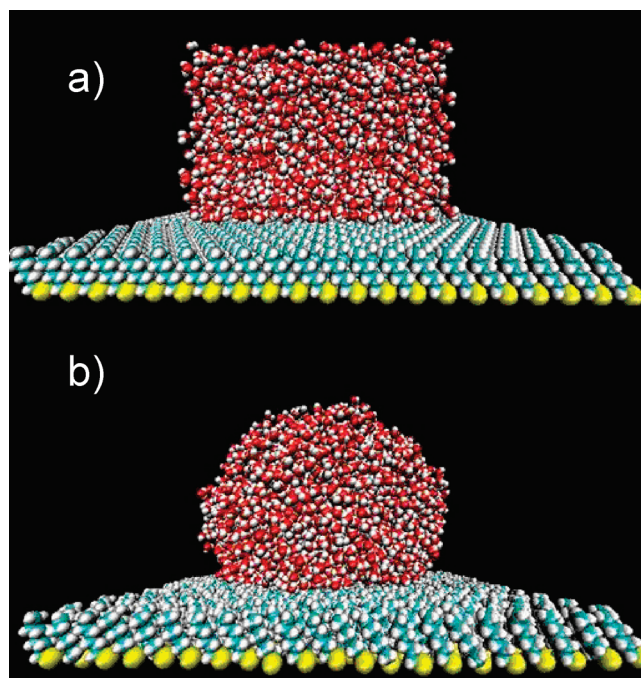


Figure 1. Snapshots of a simulated water nanodroplet on a SAM surface. (a) The initial water block at $t = 0$ and (b) an equilibrated nanodroplet at $t = 0.5 \text{ ns}$.

To investigate the hydrophobicity of the SAM surfaces that we have selected in our studies, we have performed MD simulations of nanoscopic water droplets (~ 2500 water molecules) in contact with a SAM surface of $10.5 \times 10.5 \text{ nm}^2$ area from which we have calculated the contact angle. We have used a methodology similar to that used by Debenedetti et al.^{50,52,70} to calculate the contact angle between the water droplet and the surface. Figure 1a shows an initial snapshot of the simulations and Figure 1b is an equilibrated snapshot during the simulation that clearly shows that the SAM surface used in this work is hydrophobic. Quantitatively, the calculated contact angle is 132° at 300 K employing the TIPSP water model and a hexanethiol SAM. This result is in very good agreement with the result by Dalvi and Rossky (129°),⁷¹ using a dodecanethiol surface and a water droplet of approximately the same size as that used in this work, but modeled with the SPC/E potential. These authors used a slightly different calculation procedure that assumes that the droplet is spherical, but this assumption should not affect the calculated contact angles. The agreement of our results with those in prior work lends confidence to the potentials used in our calculations. Interestingly, both calculations slightly overestimate the contact angle measured in macroscopic experiments.⁷² A potential explanation for this difference is the fact that experimental SAMs commonly contain defects at the gold surface and are composed of multiple alkanethiol domains rotated with respect to one another that give rise to frequent domain boundaries. None of these imperfections have been simulated in this work.

Additional calculations were performed for a shorter-chain, reduced-dimensionality model of the surface consisting of just the ethane termini of the hexanethiol SAM. The ethane molecules have the C atoms frozen to their positions in regular SAM so that the average separation between the SAM chains (4.98 \AA) is maintained throughout the simulations. The contact angle of

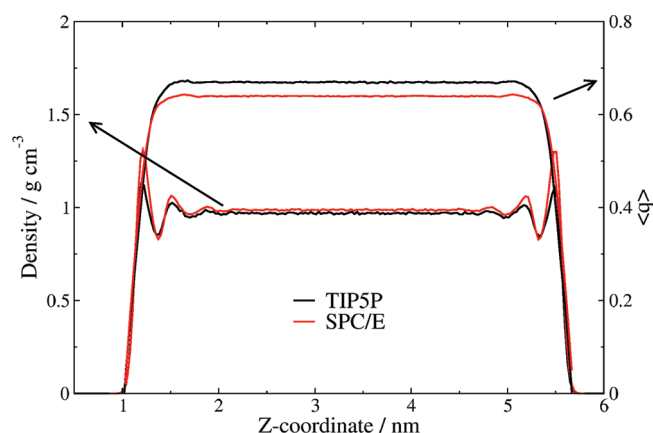


Figure 2. Density profiles and average tetrahedrality for water molecules confined between two $7.5 \text{ nm} \times 6.5 \text{ nm}$ SAM surfaces separated by 5.0 nm at 300 K . Simulation length: 10 ns . The left y-axis is for the density and the right y-axis is for the tetrahedrality.

water for this ethane surface is identical to that using the fully dimensional hexanethiol SAM, suggesting that the ethane surface is a time-saving representation of the full SAM. In the experiments referred to above, the hydrophobicity of short-chain SAMs was found to be smaller than that of longer-chain SAMs likely because surfaces made from alkanethiol molecules with less than 6 methylene units do not possess enough interchain dispersive attraction to form a regular self-assembled monolayer.⁷³ In our work, we do not see this loss of hydrophobicity with decreasing chain length because we deliberately freeze the non-hydrogen atoms by construction. The calculated contact angle provides verification that these surfaces present a hydrophobic environment in which to model the properties and dynamics of confined water.

B. Water Density and Tetrahedrality. Figure 2 shows the density of water confined between two $7.5 \text{ nm} \times 6.5 \text{ nm}$ SAM plates separated by 5.0 nm . As has been showed in various MD simulations before, the depletion layer formed between the surface and the water film originates a peak in the density of the water closest to the surface with a value well above 1 g cm^{-3} . This first peak is consequently followed by a well in the density of water below the bulk density value. This density layering continues to propagate into the water film, but as Figure 2 shows it vanishes less than 1 nm into the thin film. While the two models of water examined in this work provide different density values for the heights of the first peak, the range over which density layering can be appreciated is essentially the same.

Figure 2 also shows the degree to which the confined water experiences a tetrahedral environment as a function of its distance to the hydrophobic plates. The tetrahedrality, q , has been calculated using the standard equation⁷⁴

$$q = 1 - \frac{3}{8} \sum_{j=1}^3 \sum_{k=j+1}^4 \left(\cos(\psi_{jk}) + \frac{1}{3} \right)^2 \quad (1)$$

where ψ_{jk} is the angle formed between the vectors connecting the oxygen atom of a water molecule with the oxygen atoms of the nearest-neighbor water molecules j and k .

The figure reveals that according to this tetrahedrality metric, a hydrophobic surface does not affect dramatically the average environment experienced by water molecules. Only a slight increase in the tetrahedrality value is seen for molecules within

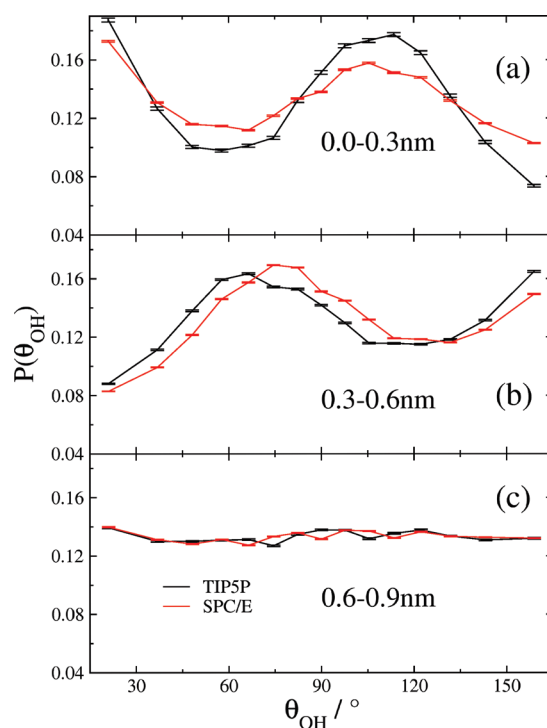


Figure 3. Distributions of the angle formed between the O–H bond vectors of water and the surface normal vector for TIP5P (black lines) and SPC/E (red) water models in the vicinity of a SAM surface in a 20 ns simulation at 300 K . Labels in each panel indicate the range of distances from the SAM surface in the water film for which the analysis is performed.

the first nanometer of the water film. Beyond that distance, water molecules experience the same environment as in bulk. Noticeably, TIP5P water is more tetrahedral than SPC/E at ambient conditions, and this result seems correlated to the higher and more accurate freezing-point temperature predicted by this model.

C. Interfacial Orientation. The orientation of water molecules at the water/surface interface provides another measure to describe the degree of hydrophobicity of a surface. In 1984, Lee et al. showed that water confined near a flat hydrophobic wall tends to orient itself in such a way as to have one of its O–H bond vectors pointing directly toward the hard-wall surface.³⁸ This orientational structure minimizes the interactions between the water molecules and the hard wall, thereby allowing the other three hydrogen-bonding vectors to actively engage in attractive interactions with either interfacial water molecules or water molecules deeper into the film. A decade later, Lee and Rossky showed that the exact opposite case is true for hydrophilic surfaces.³⁹ Simulations of water near a hydroxylated silica surface showed that one of the O–H bonds preferentially points away from the surface, allowing the other three hydrogen bonding vectors to interact with hydroxyl groups on the surface. Using a similar confining surface, Giovambattista et al. have shown that as they vary the local dipole moment of hydroxyl sites on the silica surface, there is a smooth transition from hydrophobic to hydrophilic character that can be monitored by the orientational structure of water at the interface.⁷⁰ This smooth transition in orientational structure provides a metric by which the relative hydrophobicity of the confining surface and its range into the water film can be probed for a given water model.

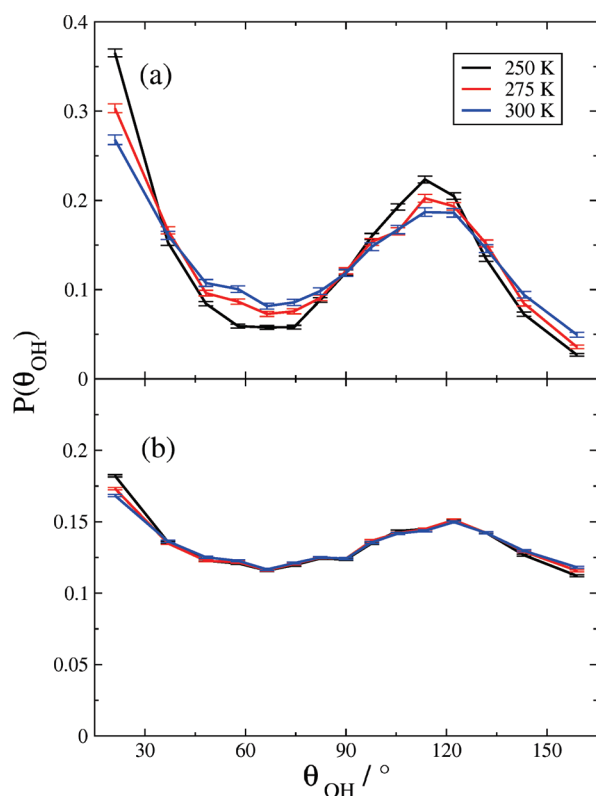


Figure 4. Distributions of the angle formed between the O–H bond vectors of water and the surface normal vector for water in the vicinity of a SAM surface in a 10 ns simulation over a range of temperatures for the (a) TIPSP and (b) SPC/E water models.

Figure 3 shows the distribution of the angle formed by the O–H bond vectors of water and the SAM surface normal over a range of distances from the surface for a 20 ns simulation of a 5 nm thick water film confined between two hexanethiol SAMs at 300 K using both the TIPSP and SPC/E water models. To better understand the range of the effect of SAM hydrophobic surfaces on water films, for the remainder of this paper we set the zero of the axis that determines the separation of a water molecule from the surface (z -axis) to the coordinate of the terminal carbon atoms on the SAM surface in that axis. Figure 3a shows the orientations of water in the layer that is closest to the surface (0–0.3 nm separation). The figure indicates a strong propensity for the water molecules to orient themselves with one of their O–H bonds pointing toward the surface, while the other O–H bond points back into the water film to establish hydrogen bonds. This result is true for both water models investigated, but the propensity for interfacial ordering is more pronounced for the TIPSP water model. The next water layer (0.3–0.6 nm) shows water molecules preferentially located in a complementary orientation to those in the interfacial layer. Molecules in this layer form a slightly enhanced hydrogen-bonding network with the interfacial layer when compared with bulk water. However, the height of the peaks in the distribution is slightly smaller than in the interfacial domain, suggesting a small loss in the anisotropy of the orientation distribution. The third layer (0.6–0.9 nm) shows a largely isotropic distribution, implying no preference for any particular orientation of O–H bond vectors relative to the surface. (This result is consistent with further analysis at longer distances from the surface.) Therefore, while the hydrophobic

SAM surface has a dramatic effect on the orientation of water close to the surface, its effects disappear well before reaching a depth of 1 nm within the film. The lack of preferred O–H bond orientations deep into the water film provides another piece of evidence from the simulations that long-range structuring does not seem like a possible explanation for the experimentally measured range of hydrophobic attraction.

To delve deeper into the water orientation near a hydrophobic surface, we have investigated angular distributions like those presented in Figure 3 as a function of temperature for both water models studied. Figure 4 shows the angular distribution for the layer of water molecules in direct contact with the SAM surface for three temperatures. The total film thickness of these simulations is 5.0 nm. Over the range of temperatures studied, the interfacial distributions are all qualitatively similar. However, the distributions become more sharply peaked with decreasing temperature, indicating an increased orientation that seems associated with a reduction in thermal motion. The temperature has a more noticeable effect for TIPSP than for SPC/E, likely because the freezing point of TIPSP water is in the temperature range studied, but that of SPC/E is much lower.

D. Diffusion Coefficients. Until now, we have analyzed the effect that a hydrophobic surface has on the structure of vicinal water. We now focus on the effect of the surface on the dynamics of water. Of course, one consequence of the vacuum region or depletion layer that forms at interface between water and extended hydrophobic surfaces is the presence of mobile water molecules. To shed light on the dynamics of these water molecules, we have calculated their diffusion coefficient in a plane parallel to the hydrophobic plates as a function of their proximity to the surface. Hereafter, we will refer to this lateral diffusion coefficient as D_{xy} . The diffusion coefficients are calculated by means of a modified version of the Einstein relationship, full details of which can be found in ref 75. Briefly, we calculate the survival probability, $P(\tau)$, for molecules that are located in a given slab of the water thin film for a period of time τ

$$P(\tau) = \frac{N(0, \tau)}{N(0)} \quad (2)$$

where N is the number of molecules in the slab. Molecules that enter the box after the initial time step or leave the box and return are not considered in the analysis. We then calculate the mean-squared change in water positions in the xy -plane, which is parallel to the hydrophobic surface

$$\langle \Delta r_{xy}(\tau)^2 \rangle_{R_k} = \frac{1}{N(0)} \sum_{i \in R_k} [(x(\tau) - x(0))^2 + (y(\tau) - y(0))^2] \quad (3)$$

Where R_k represents the set of molecules that remain in a particular slab centered at a distance z from the surface from time $t = 0$ through $t = \tau$. The diffusion coefficients are then calculated using

$$D_{xy}(z) = \frac{\langle \Delta r_{xy}(\tau)^2 \rangle_{R_k}}{4\tau P(\tau)} \quad (4)$$

For this work, we have chosen a value of $\tau = 6$ ps and water slabs of 0.35 nm thickness in the z -direction. Operationally, these values need to be balanced with the total simulation time (10 ns in our case) to provide the desired level of precision,

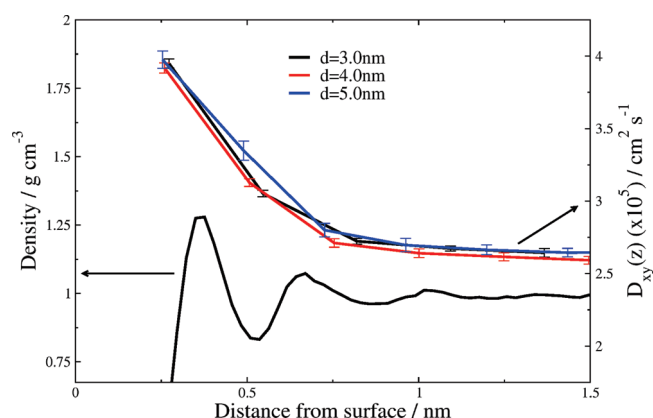


Figure 5. Density profile and diffusion coefficients parallel to the surface for TIPSP water films confined between SAMs as a function of distance from the hydrophobic surface in 10 ns simulation at 300 K. The left y-axis is for the density and the right y-axis is for the diffusion coefficients. The density profile corresponds to the 5 nm film.

since thinner slabs and longer values of τ both decrease the survival probability.

In Figure 5, we present parallel diffusion coefficients for various thin films of TIPSP water as a function of the distance from the hydrophobic layer at 300 K. The results show that water closest to the hydrophobic surface moves substantially faster than water more removed from the interface. The figure also shows that this fast lateral motion of water persists relatively deeper into the water film than the prior structural metrics described earlier in this paper. In effect, the diffusion coefficients of the confined water do not become independent of the distance from the surface until approximately 1.5 nm separation from the surface.

Using similar arguments, Romero-Vargas Castrillón et al. have recently described the length scale along which water in the proximity of a hydrophilic surface ceases to exhibit characteristics that are distinguishable from bulk.⁴² These authors have shown that there is depressed lateral translational dynamics of water on the length scale where oscillations in the density profile of water occurs, but not beyond. Figure 5 also shows the density profile of water for the simulation obtained with the 5 nm thick water film simulations. Interestingly, we see that the increase in lateral diffusion coefficient of water in proximity to a hydrophobic surface extends clearly beyond the density fluctuations in the water film, which is in contrast with the results for the hydrophilic surfaces of ref 42. Therefore, it seems that for hydrophobic surfaces, the diffusion coefficients are a more sensitive probe of the range of the perturbation of water dynamics than density layering.

The results presented in Figure 5 are consistent with those of Berne and co-workers for the air–water interface⁷⁵ and also coincide with findings of Choudhury, who has noted that water confined in hydrophobic environments experiences increased lateral diffusion.⁵⁷ Choudhury has investigated the role that hydrophobic packing plays on the dynamics of confined thin films of water, but to our knowledge this is the first report of enhanced lateral diffusion as a function of distance from a hydrophobic surface. Interestingly, Malaspina et al. reported reduced total water diffusion (parallel and normal motion were not decoupled) at the interface with a finite graphene sheet.⁷⁶ This result likely highlights the role that surface roughness plays in this diffusion phenomenon.

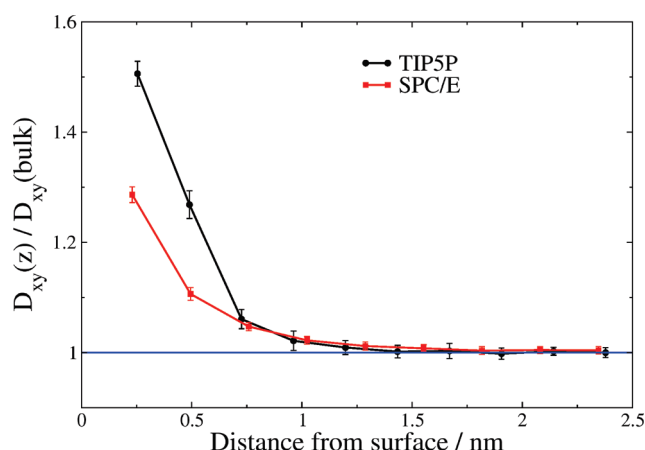


Figure 6. Parallel diffusion coefficients of two different water models as a function of the distance from the hydrophobic SAM surfaces at 300 K normalized to the bulk water diffusion coefficients for each given model. The films considered in this calculation are both 5 nm thick and the simulations were performed for 10 ns.

To examine whether the increase in water lateral diffusion coefficients by hydrophobic surfaces depends on the film thickness, Figure 5 contains the results of simulations using various water films of different sizes. As shown in the figure, the values and range of the diffusion coefficients are essentially independent of the film thickness from 3 to 5 nm thick films. In fact, only for films thinner than 2 nm we see a departure from the values in Figure 5. These results also represent an interesting difference from the previous work on hydrophilic surfaces, which found lateral diffusion coefficients to be identical for all plate separations greater than just 1.0 nm, the distance where oscillations in the density profile extend into the thin water film.

As seen in the density and tetrahedrality profiles of Figure 2, the TIPSP water model predicts a more structured water film than SPC/E at 300 K. This conclusion is consistent with the large difference in the freezing points discussed above. To analyze whether the water model influences the lateral diffusion coefficients, Figure 6 shows a comparison between the results obtained with SPC/E and TIPSP. Since the bulk diffusion coefficients of both models are different, the lateral diffusion coefficients in this figure have been normalized to their respective bulk values. The figure reveals that enhanced water mobility is predicted by both models, but the lateral diffusion coefficients predicted by the more computationally expensive TIPSP model deviate more from the bulk values than those obtained with SPC/E. On the other hand, the range of the effect of the influence of the hydrophobic surface on the diffusion coefficients is very similar for both models. In effect, Figure 6 shows that the distance at which water confined between hydrophobic surfaces behaves essentially the same as bulk water is approximately 1.5 nm for both SPC/E and TIPSP.

To further illuminate the correlation between the range of the effect of a hydrophobic surface on water structuring and on the lateral diffusion coefficients, we have investigated the temperature dependence of these metrics. Recent work by Giovambattista et al. on a film of 1.6 nm thickness indicated that reduced temperature decreases the hydrophobic nature of confining surfaces, as the depletion layer between the surface and water is narrowed.⁵² In Figure 7, we show distributions of lateral diffusion coefficients and density profiles as a function of distance from the SAM surfaces at

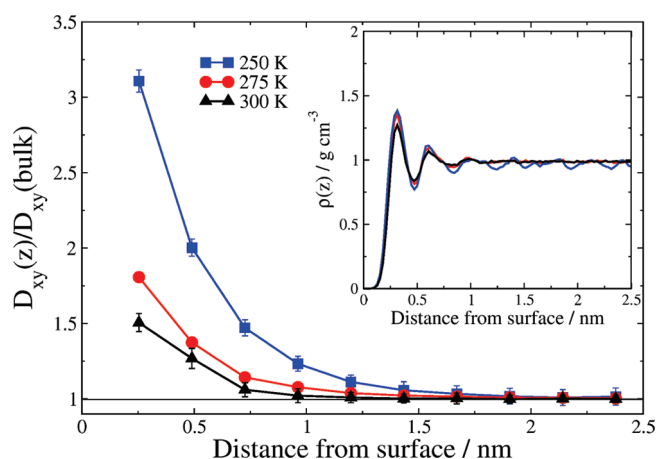


Figure 7. Parallel diffusion coefficients for TIPSP water molecules as a function of distance from the SAM surface over a range of temperatures. Diffusion coefficients are normalized to the bulk water diffusion coefficients at each given temperature. (Inset) Water density profiles for confined water as a function from SAM distance for each temperature calculated. Simulation times: 10 ns.

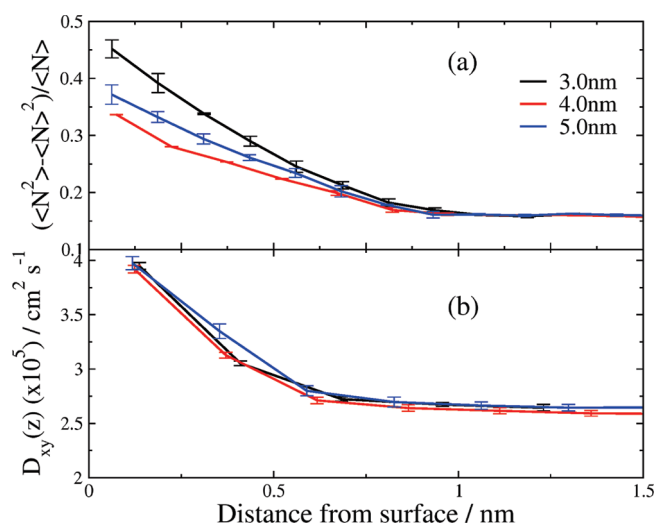


Figure 8. A comparison of the (a) density fluctuations for a spherical cavity and (b) the lateral diffusion coefficient as a function of distance from the SAM surface for three different film thicknesses of TIPSP water at 300 K. Simulation time: 10 ns.

250, 275, and 300 K for a 5 nm TIPSP water film confined between SAMs. Since the absolute value of the diffusion coefficient decreases sharply as the temperature is reduced, the distributions in Figure 7 are normalized to the bulk diffusion coefficient at each particular temperature. The figure shows that lower temperatures afford an increased range of water structuring near a hydrophobic surface. This can be ascertained from the density profiles, which show oscillations that extend well beyond 1 nm from the surface at 250 K but disappear at closer distances to the surface at higher temperatures. The increased range in the effect of the hydrophobic surface on the structure of water can also be appreciated by examining the dynamics of water, as exemplified by the lateral diffusion coefficients. As Figure 7 shows, lower temperatures both increase the values of the diffusion coefficients at a particular distance from the surface and extend the range in which water has

enhanced mobility to longer distances from the surface. These results provide an enhancement to the recent work of Giovambattista et al.⁵² on thinner water films in that the larger structuring that occurs at lower temperatures actually increases the range to which hydrophobic surfaces can influence an intervening water layer.

Finally, our MD study shows a connection between the lateral diffusion coefficients of water and the density fluctuations that have been recently described by Garde and co-workers to quantify the degree to which a surface is hydrophobic.^{46,56,77–80} The Garde group has shown that for a spherical cavity near a hydrophobic surface, the degree to which water density in that sphere fluctuates in time directly corresponds to the degree of hydrophobicity of the surface. In this work, we find that the length scale of these density fluctuations for a sphere with radius of 7.5 Å actually is remarkably similar to that of the lateral diffusion coefficient enhancement just described. Figure 8 shows this comparison between the density fluctuations and the lateral diffusion coefficients for films of thicknesses in the 3–5 nm range. The correlation between the density fluctuations and lateral diffusion coefficients provides evidence that the former can be explained by the enhanced motion of water molecule in the vicinity of a hydrophobic surface, as quantified by the diffusion coefficients. An important note is that density fluctuations are not able to discern whether the density changes emerge from water moving perpendicularly to the surface or parallel to it. The lateral diffusion coefficients reported in this work add the important detail to the knowledge drawn by the calculation of density fluctuations that turbulent behavior of water near hydrophobic surfaces has a non-negligible component emerging from enhanced water motion parallel to the surface.

CONCLUSION

We have investigated the extent to which hydrophobic confinement can influence both the structure and dynamics of water via molecular-dynamics simulations. In agreement with previous work, we have shown that hydrophobic alkanethiol SAM surfaces perturb the density profile and tetrahedrality of water in direct contact with the surface. The hydrophobic SAMs also favor an orientation of water molecules with O–H bonds pointing toward the surface. However, this work reveals that all of these structural effects are relatively short-ranged, and do not extend very far into the thin water film, that is, less than 1 nm at room temperature.

Regarding water dynamics, we have shown that the lateral diffusion coefficient of water near hydrophobic plates is enhanced with respect to bulk water. Interestingly, this enhanced motion of water extends deeper (>1 nm) into the film than any other metric of hydrophobicity we have examined in this work. Lower temperatures increase the range of the effect of the surface on the water film.

Finally, we have also shown that the enhanced water mobility in a direction parallel to the surface seems to correlate directly with the density fluctuations that have thoroughly been studied by Garde and co-workers.

A somewhat dissatisfying conclusion of this work is that even if the simulations reveal that the effect of a hydrophobic surface on the dynamics of water extends further than previously thought from MD simulations, the range of the effect is still about 2 orders of magnitude smaller than seen in the experiment. Notwithstanding, the turbulent behavior of water near hydrophobic surfaces

seen in this work might lend support to one of the disputed theories that try to explain the range of interaction between hydrophobic plates: bubble formation. In effect, the enhanced water motion described in this paper, coupled with the dissolved gas bubbles that are known to form on hydrophobic surfaces in aqueous environments,⁸¹ could provide precursor events that are responsible for bridging-bubble formation in experimental investigations of the hydrophobic effect. This effect could be further exacerbated by the imperfect nature of common hydrophobic surfaces used in the experiment, such as alkanethiol SAMs on gold. Steps, vacancies, and boundaries between alkanethiol domains, which are rotated with respect to one another, could indeed provide nucleation sites for bubble formation. Since the hydrophobic surfaces used in theoretical work lack those imperfections, in the future it will be interesting to learn how the presence of common defects in the hydrophobic surfaces affect the results of the simulations.

AUTHOR INFORMATION

Corresponding Author

*E-mail: troya@vt.edu. Phone: (540) 231-1381. Fax: (540) 231-3255.

ACKNOWLEDGMENT

This work has been supported with funding by the National Energy and Technology Lab of DOE and by NSF Grant CHE-0741927. D.T. is a Cottrell Scholar of Research Corporation.

REFERENCES

- (1) Luo, P. Z.; Baldwin, R. L. *Proc. Natl. Acad. Sci. U.S.A.* **1999**, 96, 4930.
- (2) Parthasarathy, R.; Chaturvedi, S.; Go, K. *Proc. Natl. Acad. Sci. U.S.A.* **1990**, 87, 871.
- (3) Scheraga, H. A. *J. Biomol. Struct. Dyn.* **1998**, 16, 447.
- (4) Collins, M. D.; Quillin, M. L.; Hummer, G.; Matthews, B. W.; Gruner, S. M. *J. Mol. Biol.* **2007**, 367, 752.
- (5) Collins, M. D.; Hummer, G.; Quillin, M. L.; Matthews, B. W.; Gruner, S. M. *Proc. Natl. Acad. Sci. U.S.A.* **2005**, 102, 16668.
- (6) Peters, J.; Baumeister, W.; Lupas, A. J. *Mol. Biol.* **1996**, 257, 1031.
- (7) Yin, H.; Hummer, G.; Rasaiah, J. C. *J. Am. Chem. Soc.* **2007**, 129, 7369.
- (8) Huber, G.; Mantz, H.; Spolenak, R.; Mecke, K.; Jacobs, K.; Gorb, S. N.; Arzt, E. *Proc. Natl. Acad. Sci. U.S.A.* **2005**, 102, 16293.
- (9) Kalra, A.; Garde, S.; Hummer, G. *Eur. Phys. J. - Spec. Top.* **2010**, 189, 147.
- (10) Israelachvili, J.; Pashley, R. *Nature* **1982**, 300, 341.
- (11) Parker, J. L.; Claesson, P. M.; Attard, P. *J. Phys. Chem.* **1994**, 98, 8468.
- (12) Verwey, E. J.; Overbeek, J. T. G. *Theory of the Stability of Lyophobic Colloids*; Elsevier: New York, 1947.
- (13) Derjaguin, B.; Landau, L. *Prog. Surf. Sci.* **1993**, 43, 30.
- (14) Christenson, H. K.; Claesson, P. M.; Pashley, R. M. *Proc. Natl. Acad. Sci. U.S.A.* **1987**, 98, 379.
- (15) Rabinovich, Y. I.; Derjaguin, B. V. *Colloids Surf.* **1988**, 30, 243.
- (16) Kekicheff, P.; Spalla, O. *Phys. Rev. Lett.* **1995**, 75, 1851.
- (17) Wood, J.; Sharma, R. *Langmuir* **1995**, 11, 4797.
- (18) Fielden, M. L.; Hayes, R. A.; Ralston, J. *Langmuir* **1996**, 12, 3721.
- (19) Hato, M. *J. Phys. Chem.* **1996**, 100, 18530.
- (20) Karaman, M. E.; Ninham, B. W.; Pashley, R. M. *J. Phys. Chem.* **1996**, 100, 15503.
- (21) Tamayo, J.; Garcia, R. *Langmuir* **1996**, 12, 4430.
- (22) Yaminsky, V. V.; Ninham, B. W.; Christenson, H. K.; Pashley, R. M. *Langmuir* **1996**, 12, 1936.
- (23) Yaminsky, V.; Jones, C.; Yaminsky, F.; Ninham, B. W. *Langmuir* **1996**, 12, 3531.
- (24) Bar, G.; Thomann, Y.; Brandsch, R.; Cantow, H. J.; Whangbo, M. H. *Langmuir* **1997**, 13, 3807.
- (25) Kuhle, A.; Sorensen, A. H.; Bohr, J. *J. Appl. Phys.* **1997**, 81, 6562.
- (26) Carambassis, A.; Jonker, L. C.; Attard, P.; Rutland, M. W. *Phys. Rev. Lett.* **1998**, 80, 5357.
- (27) Craig, V. S. J.; Ninham, B. W.; Pashley, R. M. *Langmuir* **1998**, 14, 3326.
- (28) Preuss, M.; Butt, H.-J. *Langmuir* **1998**, 14, 3164.
- (29) Considine, R. F.; Hayes, R. A.; Horn, R. G. *Langmuir* **1999**, 15, 1657.
- (30) Craig, V. S. J.; Ninham, B. W.; Pashley, R. M. *Langmuir* **1999**, 15, 1562.
- (31) Haugstad, G.; Jones, R. R. *Ultramicroscopy* **1999**, 76, 77.
- (32) Ishida, N.; Sakamoto, M.; Miyahara, M.; Higashitani, K. *Langmuir* **2000**, 16, 5681.
- (33) Ishida, N.; Kinoshita, N.; Miyahara, M.; Higashitani, K. *J. Colloid Interface Sci.* **1999**, 216, 387.
- (34) Ishida, N.; Inoue, T.; Miyahara, M.; Higashitani, K. *Langmuir* **2000**, 16, 6377.
- (35) Christenson, H. K.; Claesson, P. M. *Adv. Colloid Interface Sci.* **2001**, 91, 391.
- (36) Huang, X.; Margulis, C. J.; Berne, B. J. *Proc. Natl. Acad. Sci. U.S.A.* **2003**, 100, 11953.
- (37) Eriksson, J. C.; Ljunggren, S.; Claesson, P. M. *J. Chem. Soc., Faraday Trans. 2* **1989**, 85, 163.
- (38) Lee, C.-Y.; McCammon, J. A.; Rossky, P. J. *J. Chem. Phys.* **1984**, 80, 4448.
- (39) Lee, S. H.; Rossky, P. J. *J. Chem. Phys.* **1994**, 100, 3334.
- (40) Hummer, G.; Rasaiah, J. C.; Noworyta, J. P. *Nature* **2001**, 414, 188.
- (41) Choudhury, N.; Pettitt, B. M. *J. Am. Chem. Soc.* **2007**, 129, 4847.
- (42) Romero-Vargas Castrillón, S.; Giovambattista, N. S.; Aksay, I. A.; Debenedetti, P. G. *J. Phys. Chem. B* **2009**, 113, 7973.
- (43) Loveday, J. S.; Nemes, R. J. *Phys. Chem. Chem. Phys.* **2008**, 10, 937.
- (44) Walsh, M. R.; Koh, C. A.; Sloan, E. D.; Sum, A. K.; Wu, D. T. *Science* **2009**, 326, 1095.
- (45) Chandler, D. *Nature* **2005**, 437, 640.
- (46) Godawat, R.; Jamadagni, S. N.; Garde, S. *Proc. Natl. Acad. Sci. U.S.A.* **2009**, 106, 15119.
- (47) Kumar, P.; Buldyrev, S. V.; Starr, F. W.; Giovambattista, N.; Stanley, H. E. *Phys. Rev. E* **2005**, 72, 051503.
- (48) Scheidler, P.; Kob, W.; Binder, K. *Europhys. Lett.* **2002**, 59, 701.
- (49) Mittal, J.; Hummer, G. *Faraday Discuss.* **2010**, 146, 341.
- (50) Giovambattista, N.; Rossky, P. J.; Debenedetti, P. G. *Phys. Rev. E* **2006**, 73, 41604.
- (51) Giovambattista, N.; Rossky, P. J.; Debenedetti, P. G. *Phys. Rev. Lett.* **2009**, 102, 50603.
- (52) Giovambattista, N.; Rossky, P. J.; Debenedetti, P. G. *J. Phys. Chem. B* **2009**, 113, 13723.
- (53) Zhang, L.; Goddard Iii, W. A.; Jiang, S. J. *Chem. Phys.* **2002**, 117, 7342.
- (54) Jorgensen, W. L.; Madura, J. D.; Swenson, C. J. *J. Am. Chem. Soc.* **1984**, 106, 6638.
- (55) Hautman, J.; Klein, M. L. *J. Chem. Phys.* **1989**, 91, 4994.
- (56) Jamadagni, S. N.; Godawat, R.; Dordick, J. S.; Garde, S. *J. Phys. Chem. B* **2009**, 113, 4093.
- (57) Choudhury, N. *J. Chem. Phys.* **2010**, 132, 064505.
- (58) Hess, B.; Kutzner, C.; van der Spoel, D.; Lindahl, E. *J. Chem. Theory Comput* **2008**, 4, 435.
- (59) Darden, T.; York, D.; Pedersen, L. *J. Chem. Phys.* **1993**, 98, 10089.
- (60) Hess, B.; Bekker, H.; Berendsen, H. J. C.; Fraaije, J. J. *Comput. Chem.* **1997**, 18, 1463.

- (61) Berendsen, H. J. C.; Postma, J. P. M.; van Gunsteren, W. F.; DiNola, A.; Haak, J. R. *J. Chem. Phys.* **1984**, *81*, 3684.
- (62) Bussi, G.; Donadio, D.; Parrinello, M. *J. Chem. Phys.* **2007**, *126*, 014101.
- (63) Berendsen, H. J. C.; Grigera, J. R.; Straatsma, T. P. *J. Phys. Chem.* **1987**, *91*, 6269.
- (64) Mahoney, M. W.; Jorgensen, W. L. *J. Chem. Phys.* **2000**, *112*, 8910.
- (65) Fernandez, R. G.; Abascal, J. L. F.; Vega, C. *J. Chem. Phys.* **2006**, *124*, 144506.
- (66) Sakamoto, M.; Kanda, Y.; Miyahara, M.; Higashitani, K. *Langmuir* **2002**, *18*, 5713.
- (67) Zhang, J.; Yoon, R.-H.; Mao, M.; Ducker, W. A. *Langmuir* **2005**, *21*, 5831.
- (68) Hummer, G.; Garde, S. *Phys. Rev. Lett.* **1998**, *80*, 4193.
- (69) Lum, K.; Chandler, D.; Weeks, J. D. *J. Phys. Chem. B* **1999**, *103*, 4570.
- (70) Giovambattista, N.; Debenedetti, P. G.; Rossky, P. J. *J. Phys. Chem. B* **2007**, *111*, 9581.
- (71) Dalvi, V. H.; Rossky, P. J. *Proc. Natl. Acad. Sci. U.S.A.* **2010**, *107*, 13603.
- (72) Graupe, M.; Takenaga, M.; Koini, T.; Colorado, R.; Lee, T. R. *J. Am. Chem. Soc.* **1999**, *121*, 3222.
- (73) Day, B. S.; Morris, J. R. *J. Chem. Phys.* **2005**, *122*, 234714.
- (74) Errington, J. R.; Debenedetti, P. G. *Nature* **2001**, *409*, 318.
- (75) Liu, P.; Harder, E.; Berne, B. J. *J. Phys. Chem. B* **2004**, *108*, 6595.
- (76) Malaspina, D.; Schulz, E.; Alarcón, L.; Frechero, M.; Appignanesi, G. *Eur. Phys. J. E* **2010**, *32*, 35.
- (77) Shenogina, N.; Godawat, R.; Keblinski, P.; Garde, S. *Phys. Rev. Lett.* **2009**, *102*, 156101.
- (78) Sarupria, S.; Garde, S. *Phys. Rev. Lett.* **2009**, *103*, 37803.
- (79) Jamadagni, S. N.; Godawat, R.; Garde, S. *Langmuir* **2009**, *25*, 13092.
- (80) Coridan, R. H.; Schmidt, N. W.; Lai, G. H.; Godawat, R.; Krisch, M.; Garde, S.; Abbamonte, P.; Wong, G. C. L. *Phys. Rev. Lett.* **2009**, *103*, 237402.
- (81) Ducker, W. A. *Langmuir* **2009**, *25*, 8907.